A Theoretical Study of the Electronic and Optical Properties of the Graphite Intercalation Compound $K(NH_3)_4C_{24}$

Leonardo Bernasconi and Paul A. Madden*

Physical and Theoretical Chemistry Laboratory, Oxford University, South Parks Road, Oxford OX1 3QZ, U.K.

Received: April 10, 2002; In Final Form: September 19, 2002

The electronic properties of the ternary potassium−ammonia graphite intercalation compound $K(NH_3)_4C_{24}$ are studied using generalized gradient-corrected density functional theory, following recent theoretical and experimental studies on the microscopic structure and dynamics of intercalation compounds of similar composition. Localized electronic states in the intercalant $K-NH_3$ layer, whose existence has been postulated in order to explain peculiar features in the optical absorption of $K(NH_3)_xC_{24}$ compounds with $x \simeq 4$ and, ultimately, the occurrence of a 2D metal−nonmetal transition at $x \simeq 4.3$, are shown to originate from the overlap of diffuse $K-NH_3$ hybrid orbitals enveloping discrete $K(NH_3)_4$ clusters. This gives rise to a highly inhomogeneous conduction band extending in the inter-cluster region, which percolates throughout the crystal in narrow winding channels bounded by H atoms. The estimated frequency-dependent complex dielectric function is found to reproduce with remarkable accuracy the experimental spectra. In particular, we can establish a direct link between the intercalate state and the occurrence of the 1.85 eV peak in the $\epsilon_2(\omega)$ spectrum, a well-known feature specific to $K-NH_3$ graphite intercalation compounds. Issues related to the actual occupation of the intercalate state (depending on the degree of charge back-transfer from the C sheets to the $K-NH_3$ intercalate) are discussed within the limitations of a conventional electronic structure density functional approach.

I. Introduction

The existence of localized electronic states in the ternary potassium−ammonia graphite intercalation compounds (GICs) $KC_{24}(NH_3)_x$, analogous to solvated electrons in metal−ammonia solutions,[1] is one of the key features in the model proposed to explain the occurrence of the composition-induced 2D metal-nonmetal transition which is observed at $x \simeq 4.3$.[2] The binary compound KC_{24} ($x = 0$) is metallic, owing to a complete transfer of the K 4*s* electron to the highly mobile states of the carbon π^* conduction band.[3] Intercalation of NH_3 molecules is accompanied by a drop in the overall conductivity parallel to the carbon planes, which is interpreted[2] as arising from a *back-donation* of electronic charge from the graphite layers to lower mobility states localized within the $K(NH_3)_x$ intercalate. When a threshold *areal* critical charge ρ_c is reached in the intercalant, distinct states may overlap and give rise to a 2D conduction band, with a consequent rise in the in-plane conductivity. In analogy with 3D metal−ammonia solutions, this transition satisfies the 2D Mott criterion

$$\rho_c^{1/2} a_h = A \tag{1}$$

where a_h is the effective Bohr radius for the system and $A \simeq 0.31$.[2]

Optical measurements[4] provide strong support for this model. In particular, the occurrence of a sharp band in the frequency-dependent complex dielectric function located at $\hbar\omega = 1.85$ eV (similar to the peak observed at $\hbar\omega = 0.8$ eV in metal−ammonia solutions) and the sudden drop of the associated oscillator strength between $x = 4.11$ and $x = 4.38$ present convincing arguments for the existence of localized electrons in the intercalant, with the loss of oscillator strength marking the transition to the delocalized regime.

The analogy between 3D alkali metal−ammonia solutions and potassium−ammonia graphite intercalates may be helpful in devising a qualitative model for the structure of the localized states in the intercalates at $x \simeq 4$. As potassium is dissolved in liquid ammonia, the 4*s* electron is expelled into the solvent and octahedrally coordinated $K(NH_3)_6^+$ species are formed, with NH_3 molecules pointing their dipoles away from the metal center, while the free electron is transferred to solvation cages consisting of four to six ammonia molecules.[5−9] The binding of the cation to ammonia molecules is explained by charge−dipole interactions, while the comparatively lower stability of the electron cages arises from both short-range electron−dipole interactions and from long-range polarization of the NH_3 medium. If the metal concentration is sufficiently high (larger than ≃4 mol % metal), significant overlap between the wave functions of electrons belonging to different cages can occur and electron "hopping" between different cages can take place. This behavior is gradually brought about, when the metal concentration is increased, by some electrons being forced to occupy the conduction band, since too high a $K-NH_3$ ratio prevents them from residing in solvation cages.

Some important differences should be borne in mind when carrying this picture over to the intercalated potassium−ammonia liquids. In the first place, the confinement of the NH_3 molecules between the graphite layers imposes severe constraints on the structure of the intercalant with respect to 3D ammonia solutions, not only allowing only K/NH_3 monolayers to form within the galleries (preventing octahedral coordination of K^+ from occurring), but also, under the assumption of perfect periodicity in the lattice, imposing an upper bound on the maximum amount of ammonia stacked in the free space between

* Corresponding author.

10.1021/jp020946q CCC: $22.00
Published on Web 11/23/2002

the layers. The number of ammonia molecules in the unit cell (preferentially coordinated to K^+) may thus not be enough to create "true" solvation sites (defined by noncoordinated "spacing" NH_3 molecules) for the electrons back-transferred from the graphite layers. Second, the residual charge density in the highly delocalized π^* states of graphite may itself play a role in shaping the actual spatial distribution of the electrons in the intercalant states.

We have recently investigated the static and dynamic properties of several binary and ternary potassium and potassium−ammonia GICs using first-principle molecular dynamics simulations, based on generalized gradient corrected density functional theory electronic structure calculations.[10] In agreement with recent out-of-plane time-of-flight neutron diffraction studies,[11] we found roughly symmetrical ($d_{K-N} \simeq 1.9$ Å) square-pyramidal $K(NH_3)_4^{(+)}$ clusters to exist as stable species in the intercalates near $x = 4$ up to $T \simeq 600$ K, diffusing in the graphite galleries without K hopping events occurring on the few picosecond scale. At this composition, *all* the available NH_3 molecules are therefore coordinated to K^+. On the other hand, $x \simeq 4$ corresponds to the maximum of the resistance vs composition isotherm at 300 K for potassium−ammonia intercalates,[2] with a conductivity which is nearly five times smaller than in the unammoniated species. This suggests that the electrons are indeed back-transferred from the graphite states into the intercalant, but they are hindered in their free motion by some mechanism, like the confinement in localized "solvation" sites of some kind. No direct evidence has, however, been put forward so far for the occurrence of such poorly conductive intercalant states and their relation with the aforementioned features in the absorption spectrum.

The work described in this paper is an investigation into the nature of the electronic states in the interlayer region of the intercalation compound $K(NH_3)_4C_{24}$, and it is aimed at characterizing their origin, shape, spatial extent, and localization properties. As a direct consequence of the results of refs 10 and 11, we approach the problem by considering how an electron distributes in space around $K(NH_3)_4^+$ units, from a single isolated cluster in the gas phase to a condensed 2D crystal phase representative of the intercalant $K(NH_3)_4$ layer in the full GIC. The electron is found to reside in a hybrid state originating from mixing of K atomic and NH_3 antibonding orbitals. Overlap of extended hybrid states from different $K(NH_3)_4^+ \cdot e^-$ units leads to the formation of a 2D band extending in the intercluster region and delimited by H atoms of different NH_3 molecules. This extended state is conserved essentially unchanged when the hypothetical 2D phase is confined between carbon layers in the atomic arrangement which has been determined for the 0 K structure of the $K(NH_3)_4C_{24}$ GIC,[10] and manifests itself as a rather narrow (~2 eV width) band lying in the close vicinity of the Fermi energy in several points of the Brillouin zone. The imaginary part of the dielectric function is computed within the linear response approximation. Although, as will be seen below, our calculations do not provide direct information on the magnitude of charge back-transfer from the carbon bands to the intercalant layer, they fully support the involvement of the "solvated" electron band in the optical response of $K-NH_3$ GICs of composition $x \simeq 4$. In particular, we prove here that the occurrence of the 2D band in the $K-NH_3$ layer *and* its occupation are necessary conditions for the sharp 1.85 eV peak to appear in the $\epsilon_2(\omega)$ spectrum.

The paper is organized as follows. General details regarding the calculations are given in Section II, though more thorough information is provided in turn for each of the systems examined throughout the paper. A detailed analysis of the electronic structure of the $K(NH_3)_4^+ \cdot e^-$ system (the basic unit in the confined 2D $K-NH_3$ liquid within the $K(NH_3)_4C_{24}$ compound) is then presented, with particular emphasis on the changes which are brought about by varying the areal cluster density from an isolated gas-phase cluster to the density and cluster arrangement characterizing the $K-NH_3$ layer in the 0 K structure of the $K(NH_3)_4C_{24}$ GIC. The formation of an extended, highly inhomogeneous, narrow band is demonstrated and its origin is explained on the basis of simple considerations of the symmetry properties of the molecular orbitals involved. The full intercalate is analyzed in Section III. A "rigid-band" approach is used in the first place to identify the energy range of the intercalant band and to disentangle its contribution from the full band-structure of the GIC. Ignoring spin-polarization effects and partial occupation of the Kohn−Sham orbitals leads to the conclusion that this band is at least partially occupied, supporting the model for a charge back-transfer from the carbon layers. Within these assumptions, the frequency-dependent complex dielectric function is estimated and it is found to accurately reproduce the experimental spectra. Allowing for self-consistent partial occupation of the Kohn−Sham orbitals does, however, result in the intercalant band becoming unoccupied everywhere in the Brillouin zone, though the band-structure is little changed. The corresponding $\epsilon_2(\omega)$ differs from the previous system in the absence of the 1.85 eV peak mentioned above. This establishes an unambiguous relation between occupation of the intercalant band and the occurrence of this characteristic feature in the optical spectrum. The implications of these findings are discussed in Section IV and interpreted in the light of possible shortcomings of conventional (approximate) density functionals in accounting for the relative energies of localized/delocalized electron bands.

II. Details of Calculations

Kohn−Sham[12] density functional theory[13,14] electronic structure calculations were performed within the generalized gradient corrected local density approximation[15] to the exchange-correlation energy. Ion−electron interactions were described using ab initio pseudopotentials either of the norm-conserving[16−18] or ultrasoft[19] type. Norm-conserving pseudopotentials included nonlocality via the Kleinman−Bylander[20] scheme (with *s* nonlocal projectors for N and H), whereas a purely local potential was used for K. Ultrasoft pseudopotentials included *s* and *p* nonlocality for C, N, and K (with semicore 3*s* and 3*p* states explicitly treated as valence electrons) and *s* nonlocality for H. The Kohn−Sham eigenvalues were expanded in plane-waves up to a kinetic energy cutoff of 400 eV for norm-conserving and 270 eV for ultrasoft pseudopotentials. Electronic energy minimizations[21,22] were accomplished using an all-band conjugate gradient solver[21] with a Pulay charge density mixing scheme,[23] yielding a convergence in the ground-state energy not worse than 5×10^{-6} eV/atom. Integrals over the Brillouin zone were estimated by quadrature[24] using homogeneous Monkhorst-Pack grids[25] of 1 (Γ point) to 5 **k**-points, depending on the dimension and symmetry of the unit cell. From the ground-state charge densities thus obtained, Kohn−Sham energies (including up to twice as many virtual orbitals as the occupied states) over larger numbers of **k**-points were computed, which were used in the calculation of band-structures and in the estimate of the complex dielectric function.[41,42]

III. Structure and Electronic Properties of $K(NH_3)_4^+ \cdot e^-$

The structure of the free $K(NH_3)_4$ cluster was optimized adopting a periodically repeated cubic supercell of size $a = 10$

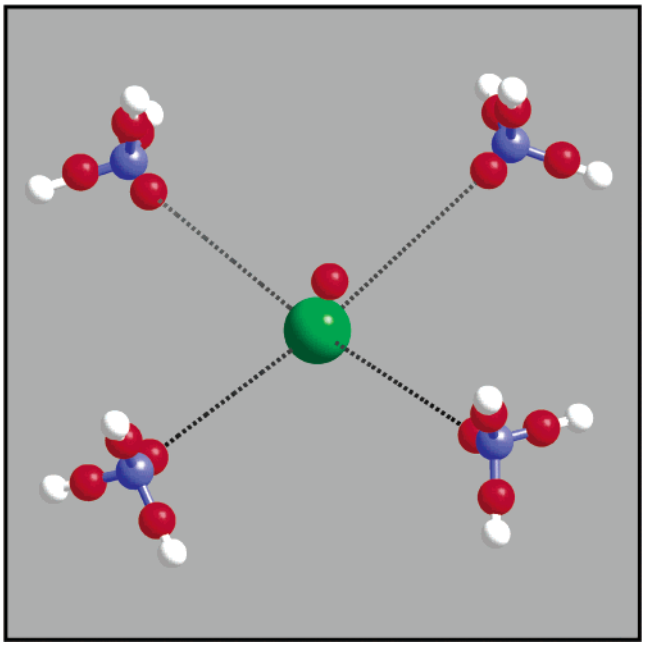

Figure 1. WFC positions in the free $K(NH_3)_4$ complex, represented by a small ball placed on the calculated position of the Wannier centers. Here, as in the following figures, the larger ball indicates K. Note the vicinity of one of the WFCs to K and their tetrahedral distribution around N.

Å. Spin polarization was explicitly taken into account and Vanderbilt ultrasoft pseudopotentials were used, with semicore 3*s* and 3*p* states of K included among the valence electrons, to allow for an accurate estimate of the interionic forces. A Broyden-Fletcher-Goldfarb-Shanno algorithm (as implemented in CASTEP 4.2) was used to locate the minimum-energy geometry, allowing atomic relaxation until the forces on the ions were lower than 0.05 eV/Å. The cluster is square-pyramidal with $d_{K-N} = 2.922 \pm 0.04$ Å, and a tilt angle of the NH_3 C_3 axis with respect to the plane defined by the N atoms of 7.72 $\pm$ 0.5°. The NH_3 molecules point their dipoles away from K^+ and they are essentially undistorted with respect to the gas phase ($d_{N-H} = 1.018$ Å, HNH = 107.39°). The optimized geometry of the *neutral* $K(NH_3)_4$ system is therefore not dissimilar from that of the $K(NH_3)_4^+$ clusters found in the intercalate. This ionic arrangement was then kept fixed in all the other electronic structure calculations on this system, which were performed using norm-conserving pseudopotentials (purely local potential for K). In addition, the system was regarded as non-spin polarized, by considering *all* the Kohn−Sham states (including the last one, which is in principle half-filled because of the odd number of electrons) as if doubly occupied. According to results of ref 10, this is not expected to introduce important changes in the electronic structure, though energies and ionic forces (not of interest here) may be slightly affected.

A full electronic structure calculation at fixed ionic positions was performed on periodically repeated orthorhombic supercells of size 14 × 14 × 10, 12 × 12 × 10, 10 × 10 × 10, and 8 × 8 × 10 Å, with the plane defined by the four nitrogen atoms roughly parallel to the *ab* face of the cell. A unitary transformation of the Kohn−Sham orbitals to maximally localized Wannier functions (MLWFs)[26−28] was then carried out, including all the occupied Kohn−Sham eigenstates. As an example, the Wannier function centre (WFC) positions for the free cluster are represented in Figure 1 for the unit cell of dimension 14 × 14 × 10 Å.

TABLE 1: Wannier Function Analysis of the NH_3 Molecule in the Free Species[a] (first line) and in the $K(NH_3)_4$ Complex at Various Supercell Parameters and Cluster Orientations (see text for details)[b]

		N-lp (Å)	$\omega_{lp}^{1/2}$ (Å)	N-σ (Å)	$\omega_\sigma^{1/2}$ (Å)	$(\omega_{lp}/\omega_\sigma)^{1/2}$	μ (D)
NH_3	10 Å	0.323	0.89	0.603	0.76	1.17	1.48
$K(NH_3)_4$	14 Å	0.336	0.63	0.576	0.54	1.17	2.00
$K(NH_3)_4$	12 Å	0.348	0.73	0.592	0.62	1.18	2.07
$K(NH_3)_4$	10 Å	0.365	0.86	0.600	0.73	1.18	2.10
$K(NH_3)_4$	8 Å	0.376	1.05	0.599	0.92	1.14	2.08
$[K(NH_3)_4]_2$	hex.sc.	0.371	0.65	0.595	0.54	1.20	1.94
$[K(NH_3)_4]_2$	GIC	0.370	0.66	0.594	0.56	1.18	1.88

[a] Ref 29. [b] hex.sc. indicates the *free* $K(NH_3)_4$ crystal in the intercalate geometry; GIC labels the full intercalate $[K(NH_3)_4]_2[C_{24}]_2$); N-lp and N−σ are distances of the WFCs corresponding to sp^3 hybrids with non-bonding (lone-pair) and bonding (σ) character from the N center; and $\omega_{lp}^{1/2}$ and $\omega_\sigma^{1/2}$ are the corresponding average MLWF spreads.

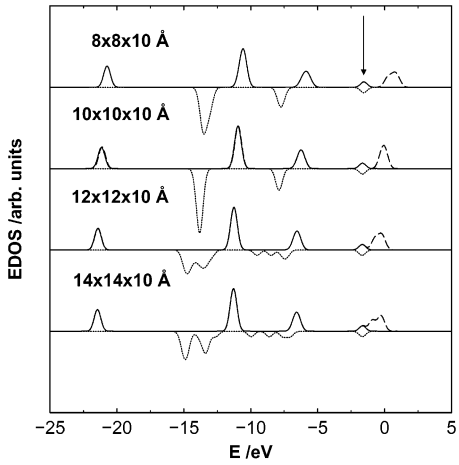

Figure 2. EDOS computed from the Kohn−Sham eigenvalues (continuous line), including 5 empty states (dashed line), compared with EDOS obtained from MLWF energy levels (dotted). The arrow indicates the energy of the HOMO. A Gaussian smearing of 0.25 eV has been introduced.

a. Wannier Function Analysis of the NH_3 Molecules. The eight valence electrons of each NH_3 molecule localize in one lone-pair and three σ-bond-like (sp^3) Wannier functions. The dipole moment of each NH_3 molecule was therefore computed from the position of the four WFCs closest to a given N atom ($Z = -2|e|$) and the nuclear pseudopotential cores ($Z_N = 5|e|$, $Z_H = |e|$). Results are summarized in Table 1. The distance from N of the WFC of the three σ bonds in each ammonia molecule increases slightly (~0.04 Å), and the lone-pair center is displaced away from N by 0.04−0.05 Å toward K^+, with respect to the free species.[29] Both these effects contribute to an increase in the dipole moment of each ammonia molecule, which is ~0.6 D larger than in the gas phase. Although the absolute value of the spread depends on the dimension of the unit cell (converging very slowly to its $L \rightarrow \infty$ limit as L is increased[26]), it is interesting to note that the *ratio* between lone-pair and σ-bond-like Wannier function spread ($\omega_n^{1/2} = (\langle r_n^2 \rangle - \langle \boldsymbol{r}_n \rangle^2)^{1/2}$) remains nearly constant (with the possible exception of the smallest supercell considered). The nature of the Wannier functions localized on the ammonia molecules is thus retained in all cases, though the absolute value of their individual spread varies with the cell size.

b. Nature and Spatial Distribution of the "Excess" Electron. The electron density of states (EDOS) calculated from the Kohn−Sham eigenvalues is shown in Figure 2, along with

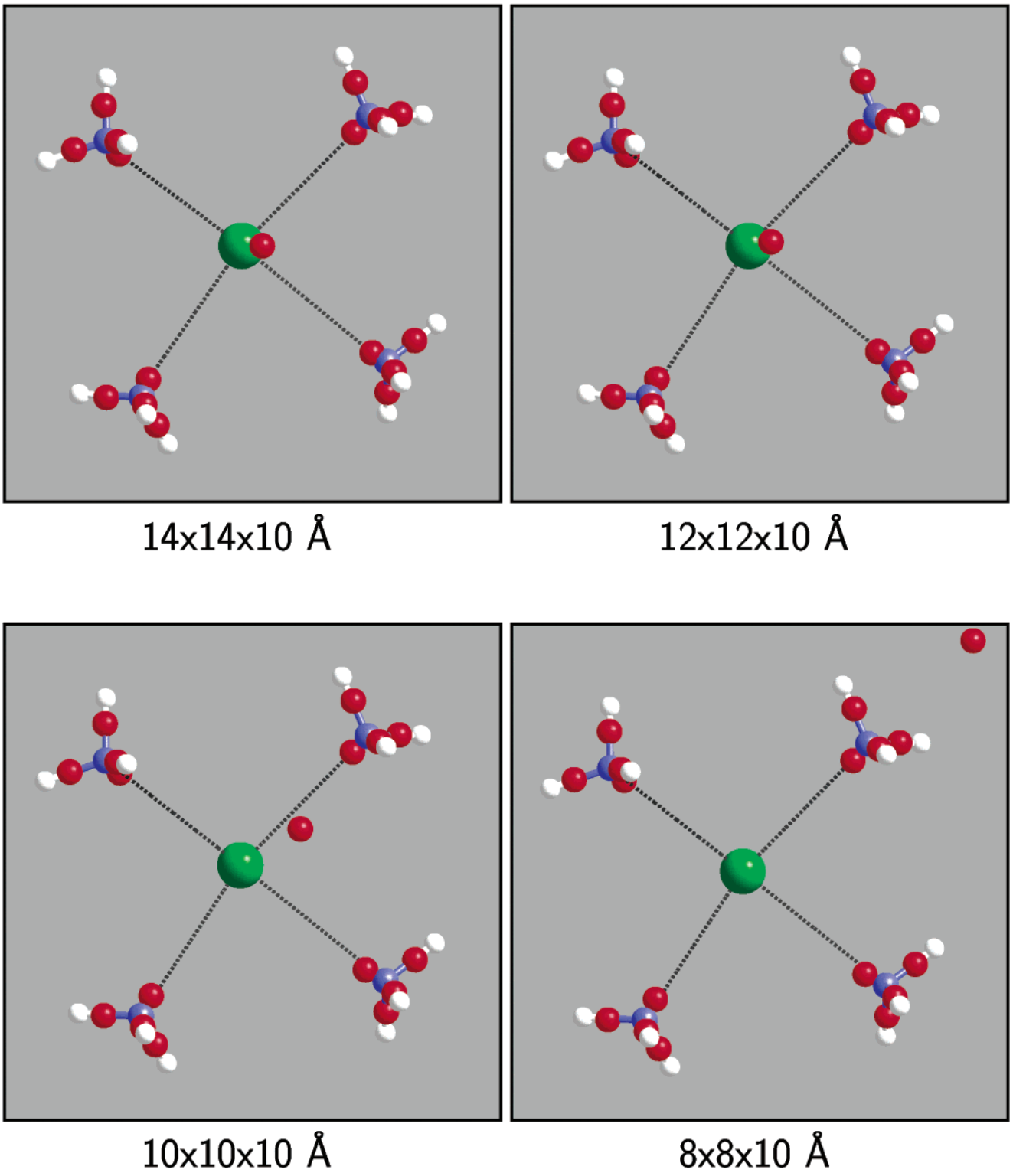

Figure 3. WFC positions at various supercell parameters. Note the shift in the position of the WFC corresponding to the highest occupied MLWF, which is close to the K^+ ion in the largest cells. See text for explanation.

the corresponding Wannier function energy levels ϵ'_i obtained from the set of occupied Kohn−Sham eigenvalues ϵ_i as[30−32]

$$\epsilon'_n = \langle w_m|\hat{H}_{KS}|w_n\rangle\delta_{nm} \equiv \sum_i U^*_{in}U_{in}\epsilon_i \qquad (2)$$

where $\hat{H}_{KS}$ is the Kohn−Sham Hamiltonian, $|w_i\rangle$ are the Wannier orbitals, and **U** is the unitary matrix which transforms the Kohn−Sham orbitals $|\phi_i\rangle$ into MLWFs,

$$|w_i\rangle = \sum_j U_{ji}|\phi_j\rangle \qquad (3)$$

The Kohn−Sham states of NH_3 (between ~ -22 and ~ -2 eV) and the corresponding Wannier states (σ-bond and non-bonding sp^3 hybrids at ~ -15 and ~ -7 eV) are well separated

in energy from the K 4*s* electron (conventionally indicated here as HOMO). The most striking change which is brought about by varying the dimensions of the unit cell is the removal of the degeneracy within the subgroups of the bonding and nonbonding Wannier orbitals at large cell sizes. This effect is not mirrored in the distribution of the Kohn−Sham eigenvalues, which only slightly displace toward lower energies. Since the Kohn−Sham states are typically delocalized over all the NH_3 molecules, while each Wannier orbital is specific to a given molecule, this result indicates that, at large cell sizes, the four ammonia molecules are no longer equivalent from the point of view of their electronic properties. The origin of this symmetry breaking within sets of hybrid orbitals with the same character may be understood by monitoring the positions of the WFCs when the simulation cell is being shrunk in the *ab* plane (Figure 3). In the free-cluster ($14 \times 14 \times 10$ Å) the center of charge of the HOMO (corresponding to the WFC position of the highest-energy Wannier orbital) is located in the vicinity of the K ion (at ∼0.792 Å), within the pyramidal hole defined by K^+ and the four N atoms. As the cell size is decreased, its distance from K^+ increases, and eventually ($8 \times 8 \times 10$ Å) the WFC leaves the coordination hole moving toward the outer region of the cluster. Increasing the cluster concentration thus creates coordination sites for the HOMO electron other than the pyramidal hole.

The migration of the HOMO center away from K suggests that a transfer of charge is taking place between the core and the outer region of the cluster. This is indeed confirmed by plotting the charge density associated with the HOMO (or of the highest energy Wannier orbital) in the free cluster (e.g., $12 \times 12 \times 10$ Å, Figure 4) and in the higher cluster density regime ($10 \times 10 \times 10$ Å, Figure 5). In the free cluster, the charge density concentrates in a rather flat area below the base of the pyramid cluster and in regions adjacent to the H atoms. The asymmetric distribution of charge may derive from the slight differences in the K−N distances among the four NH_3 molecules and can in turn remove the degeneracy between the Wannier orbitals with similar character on the ammonia molecules.

As the clusters are forced to approach each other, the charge density of the HOMO moves toward wide regions between the clusters, sometimes connected by narrow channels, and the flat concentration of charge in the vicinity of the plane defined by the N atoms tends to disappear. In this situation, degeneracies among groups of Wannier orbitals are restored, since the perturbing charge concentration in the vicinity of the ammonia molecules has been removed. It is interesting to note that each of these wide regions is bound by four (two pairs from two different supercells, Figure 6) H atoms belonging to different ammonia molecules, which may constitute an ideal "solvation" site for the electron density. Overlap between HOMO orbitals belonging to different cells takes place via superposition of solvation regions of different cells, and this gives rise to an extended state which spreads throughout the crystal by "wetting" H atoms of distinct ammonia molecules. In addition, the competition between solvation sites between clusters and in the region below the plane of the N atoms leads to the appearance of flat winding channels which can occasionally connect different solvation regions.

A distinctive geometric feature of $K(NH_3)_4$ at 0 K (Figure 1) is that all the ammonia molecules point one of their N−H bonds downward, roughly perpendicular to the plane defined by the N atoms. The corresponding H atoms thus define themselves a square solvation site (of side ≃4.2 Å), where the HOMO electron resides preferentially in the diluted cluster regime,

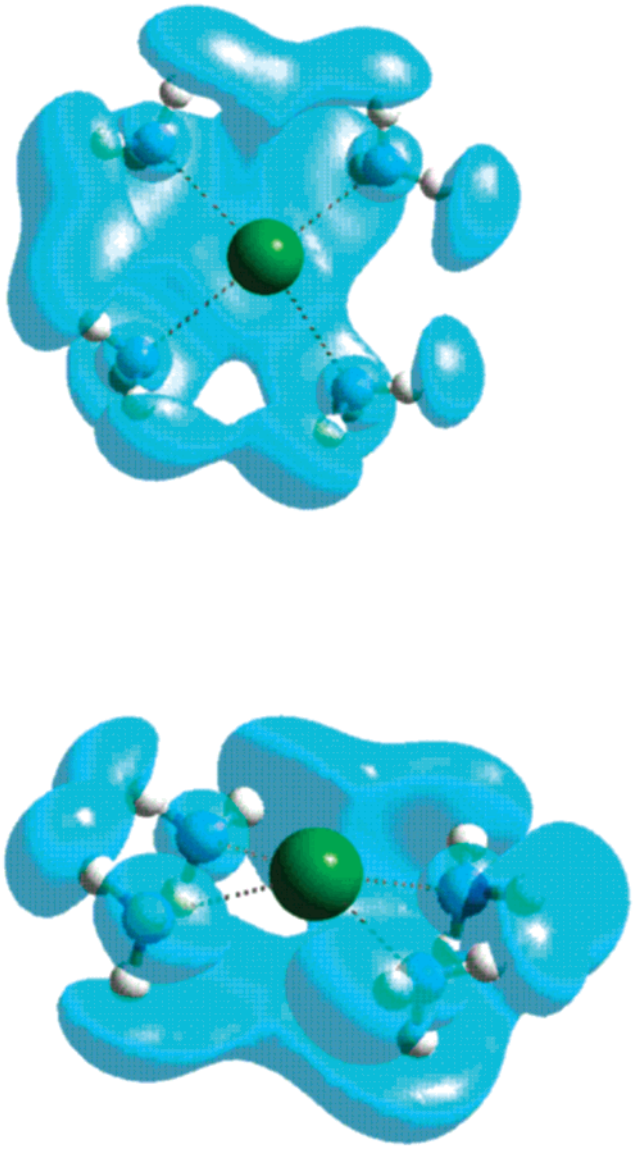

Figure 4. Charge density isosurface, corresponding to 0.0035 electrons/Å^3, from the "floating" K 4*s* state (HOMO) in $K(NH_3)_4$. The supercell (not indicated) is of size $12 \times 12 \times 10$ Å.

though part of the charge density tends to overflow and wet some of the upper H atoms (Figure 4). This facilitates the transfer of charge to new solvation sites between the clusters, which are produced when the high-density regime is approached (Figure 5). The very diffuse nature of the HOMO electron (its spread being around 9 times as large as that of a NH_3 σ-bond sp^3 hybrid) favors facile transfer between different sites and the occurrence of links between different solvation regions.

These findings may be rationalized in view of the experimental[33,34] and theoretical[35] results of studies performed on the metallic molecular crystal $Li(NH_3)_4$. In both liquid and solid phases, $Li(NH_3)_4$ is known to consist of $Li(NH_3)_4^+$ units, with NH_3 molecules tetrahedrally arranged around Li and pointing their dipoles away from it (i.e., orienting their lone-pair toward the metal atom). The Li atom hybridizes its 2*s* and 2*p* atomic orbitals, forming four sp^3 hybrid orbitals which can accommodate the NH_3 lone-pairs. The 2*s* valence electron is promoted to the empty 3*s* orbital which is stabilized by combination with the first antibonding molecular orbital (MO) of the NH_3 molecules. The in-phase overlap leads to a MO located between the hydrogen atoms (see, e.g., Figure 1 of ref 35), and the out-

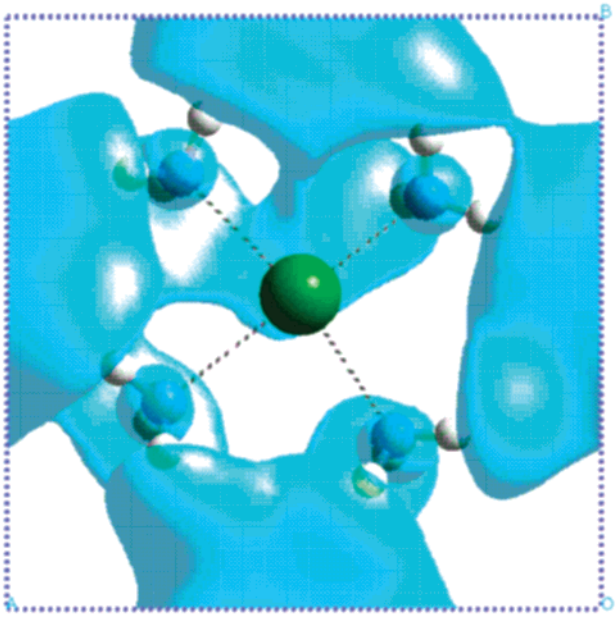

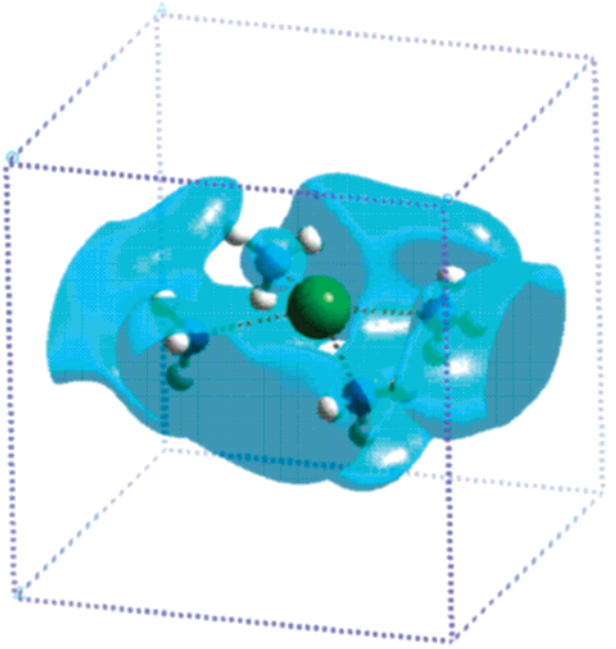

Figure 5. Charge density isosurface, corresponding to 0.0035 electrons/Å^3, from the "floating" K 4*s* state (HOMO) in $K(NH_3)_4$. The supercell (dashed lines) is of size 10 × 10 × 10 Å.

of-phase one located between the hydrogens and the nitrogen. A conduction band is thus formed, based on Li 3*s* orbitals.

A similar picture may be adopted for $K(NH_3)_4$, with the difference that low-energy 3*d* states are now available for orbital hybridization, and *s*−*p* hybridization is much less favorable. This can lead to four sp^2d hybrids, with a square-planar coordination geometry (D_{4h}), where the NH_3 lone-pairs can be accommodated. The valence electron of K, initially in the 4*s* orbital, can be promoted to the $4p_z$ or $3d_{z^2}$ orbitals not involved in the hybridization process, both of which elongate perpendicular to the plane defined by the four hybrids. This is consistent with a transition from the octahedral coordination observed in bulk K/NH_3 solutions to the square planar geometry,

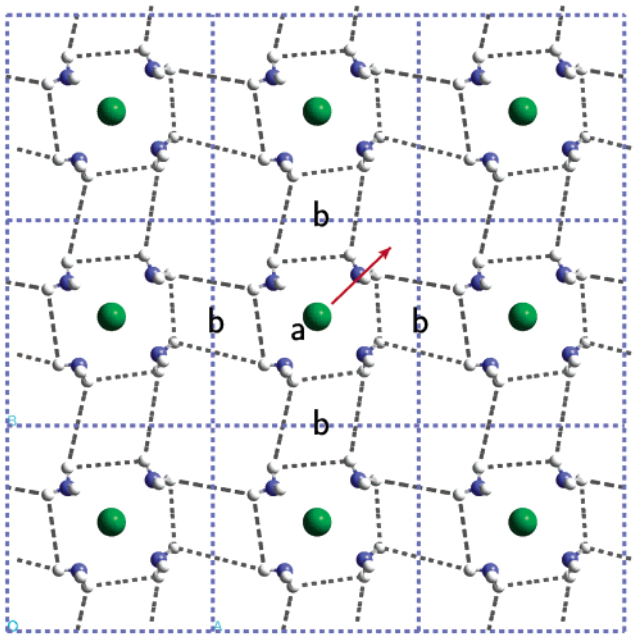

Figure 6. Artificial two-dimensional crystalline cubic arrangement of $K(NH_3)_4$ clusters (cell size 10 × 10 × 10 Å). The dark dashed lines indicate the two types of solvation sites (*intra* (a) and *inter* (b) cluster) for the "excess" electron surrounding the $K(NH_3)_4^+$ core. The arrow indicates the displacement of the HOMO WFC as the clusters are forced to approach each other because of the unit cell shrinkage.

by removal of two trans NH_3 molecules. The pyramidal distortion observed in the $K(NH_3)_4$ clusters in the optimized geometry may derive from the additional stabilization which can arise from Coulombic interaction between the H atoms of the NH_3 molecules (polarized by the coordination to the metal center) and the charge density concentrated on one side of the coordination plane. This can ideally be accomplished by including some of the character of the $4p_z$ or $3d_{z^2}$ orbitals in the hybrids and allowing the K−N bonds to bend so as to create the additional "solvation" square planar site below the basal plane of the pyramid. In addition, admixture of orbital character from antibonding MO of the ammonia molecules can explain the tendency of the HOMO charge density to concentrate partly in the outer region of the cluster, especially in the vicinity of the H atoms. The highly diffuse nature of these MOs facilitates the formation of an extended band via overlap of states from different clusters.

c. "Floating-Electron" Band in a 2D $K(NH_3)_4^+ \cdot e^-$ Crystal. It is interesting to examine how the excess electron distributes in space when the $K(NH_3)_4^+$ clusters are arranged in a 2D array analogous to the 2D $K(NH_3)_4^+$ crystalline layer in the 0 K structure of the GIC $K(NH_3)_4C_{24}$.[10] This fictitious (neutral) system may be regarded as a convenient simplified model of an intercalated $K-NH_3$ layer when a *complete* transfer of charge from the graphite sheets has occurred. Calculations on this system were performed adopting similar specifications as for the previous systems. A periodically repeated supercell of 2 × 1 × 1 hexagonal unit cells was adopted with $a = 17.04$ Å, $b = 8.52$ Å, $c = 6.65$ Å, $\alpha = \beta = 90°$, $\gamma = 60°$. The repeated formula unit was therefore $[K(NH_3)_4]_2$. Adopting a larger supercell in place of the true unit cell allowed for a reasonably accurate description of the electronic distribution to be obtained within the Γ point approximation[24] and for the errors in the iterative procedure for computing localized Wannier orbitals to be largely reduced.[26,28]

The structure of the $K(NH_3)_4$ clusters in this system is very similar to that of the free species,[10] though the K−N distances

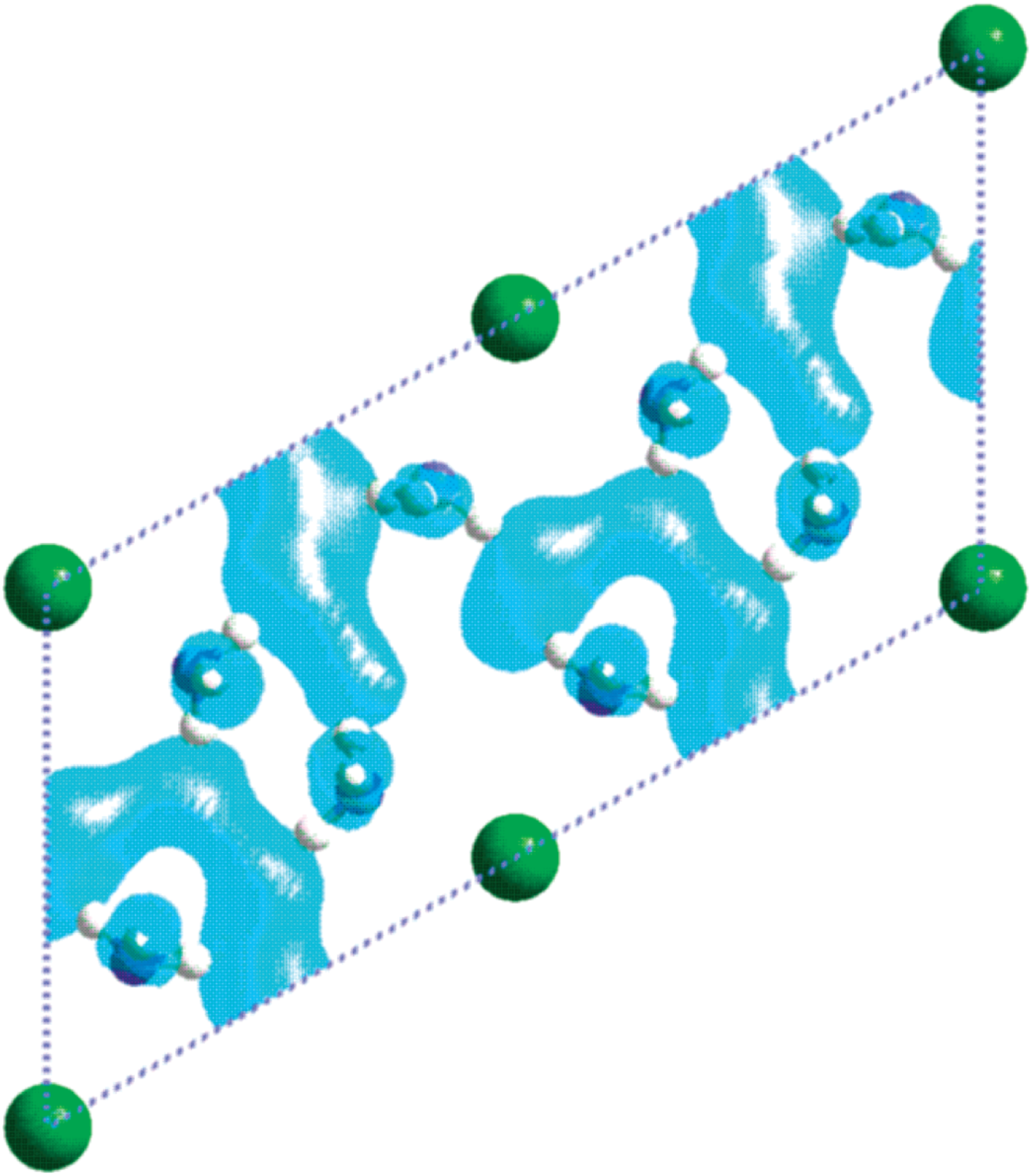

Figure 7. Charge density isosurface (0.0035 electrons/Å^3) from the last occupied band of the two-dimensional hexagonal layer $[K(NH_3)_4]_2$, as seen along the *c* axis. The *b* axis is in the vertical direction.

are typically shorter (2.828 ± 0.1 Å) and the tilt angle of the C_3 axis with respect to the plane of the N atoms is reduced to ∼5.5°. The dipole moment of NH_3 is larger (0.46 D) than in gas-phase NH_3, but slightly smaller (0.06 D) than in the free (14 × 14 × 10 Å supercell) cluster (Table 1).

The HOMO is again well separated in energy from the ammonia states, and does not mix with them during the Wannier localization procedure. Due to the noncubic unit cell shape, the total MLWF spread is a tensor with five nonzero elements,[26,28] as is the single-band spread ω_i. We therefore define the spread of a given MLWF as the sum over *all* the elements of the tensor. The ratio between the spreads of nonbonding and bonding sp^3 hybrids is close to that observed for the free clusters (Table 1), while the extended-electron MLWF (or the corresponding Kohn−Sham orbital) is found to be ∼7 times more spread than a bonding N−H orbital (to be compared with the free-clusters, whose corresponding spread ratio is ∼3).

The charge density distribution obtained from the corresponding MLWF is shown in Figure 7. As expected from the above discussion, the charge density tends to localize in narrow and

highly inhomogeneous winding channels defined by H atoms and spreading throughout the lattice. A clear tendency to avoid the intracluster region is also evident, which is indicative of a complete transfer of charge away from the cluster centers. This situation can be described as an ordered array of positive "ions" (fully ionized $K(NH_3)_4^+$ clusters) plus a 2D "floating-electron" (fe) band, analogous to the quasi-percolating electronic states predicted in solid-phase-II $Li(NH_3)_4$[35] and in molten salt solutions of composition $K_x(KCl)_{1-x}$ ($x = 0.06, 0.11$).[36] It is interesting to notice that the wider regions of high electron density are delimited by triads of hydrogens belonging to different NH_3 molecules, in qualitative agreement with the model for the structure of the solvated electron states proposed by Huang et al.[2] for K−NH_3 GICs with compositions close to the M−NM transition. Our results do, however, indicate that the participation of a spacing (non-coordinated) NH_3 molecule to the electron solvation is not strictly a requirement for such states to make their appearance, suggesting that suitable target sites for charge transfer from the carbon layers are already present at $x = 4$, with all the NH_3 molecules coordinated to K. This explains the observed maximum of the *a*-axis resistance vs x curve at (or in the very close vicinity of) $x = 4$.

d. Brillouin Zone Dispersion of the fe Band. The fluctuations in the charge density and the very clear directional character of the fe band are a direct consequence of its origin from the overlap of the HOMO of different $K(NH_3)_4$ clusters. In simple metals, such as Li and Na, the conduction band derives from overlap of *s* orbitals, which results in a highly homogeneous spatial distribution of the conduction electrons throughout the lattice. One would, therefore, expect the ability of the fe band to act as a genuine conduction band to be reduced with respect to simple metals, owing to the smaller density of charge carriers and their lower mobility. In analogy with the molecular crystal $Li(NH_3)_4$, it is therefore possible to include the system studied here in the class of the *expanded metals*, characterized by mean electronic densities in the conduction band which are 1 order of magnitude smaller than in simple metals.[35] The important difference with respect to $Li(NH_3)_4$ is that the basic units in the crystal (which replace the spherically symmetric positive ions in the simple metals) are in the present case nearly *planar* clusters (with average radius ∼3.6 Å), instead of tetrahedral molecules. This poses less severe restrictions on the condition for the phase matching of HOMO orbitals belonging to different clusters with respect to $Li(NH_3)_4$, and, in particular, it allows for the formation of a nearly two-dimensional conduction band. However, the degree of overlap between orbitals of different clusters will remain less effective than in the spherically symmetric situation, giving rise to only a *narrow* band.

To test these ideas, a full band-structure calculation was performed on the isolated $K(NH_3)_4$ layer in the same geometry as the one considered so far, but adopting the true unit cell of size $a = b = 8.52$ Å, $c = 6.65$ Å, $\gamma = 120°$ (in order to reduce the number of electronic states with respect to the previous calculation). A full self-consistent *non-spin polarized* generalized gradient-corrected DFT calculation was carried out using Vanderbilt ultrasoft pseudopotentials with *s* and *p* nonlocal projectors for K and N and *s* for H. 3*s* and 3*p* states of K were in this case explicitly treated as valence electrons. Although this was found not to affect substantially the electronic distribution near the Fermi energy, the presence of very localized low-energy states in the band-structure plot may provide a convenient reference in comparing electronic energies of related systems (see discussion in the following section). Four **k**-points were

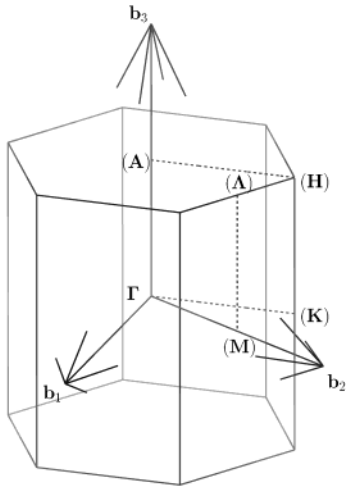

Figure 8. Brillouin zone (continuous lines), reciprocal space axes (arrows) and "high-symmetry" points used in band-structure calculations. See text for explanation.

included in the BZ sampling, namely, in scaled units, ($^1/_4$, $^1/_4$, $^1/_4$), ($^1/_4$, $^1/_4$, $-^1/_4$), ($^1/_4$, $-^1/_4$, $^1/_4$), ($^1/_4$, $-^1/_4$, $-^1/_4$), corresponding to a homogeneous Monkhorst-Pack mesh of $2 \times 2 \times 2$ points. The ground-state charge density thus obtained was used to construct the self-consistent Kohn−Sham potential, from which the electronic energies were estimated for a larger number of **k**-points, also including 10 additional empty states for each **k**-point. The BZ and the reciprocal space construct are schematically represented in Figure 8. The high symmetry points are labeled according to the conventional symbols for the space group 189 ($P\bar{6}2m$) which has been found to account for the real space symmetry properties of the compound KC_{24}.[10] In the specific case of the system under study, this choice of symmetry is obviously inappropriate, but the relevant nomenclature has been maintained in order to allow for easier comparison between different systems in the subsequent discussion. Parenthesis are used here to indicate that the labeling is purely conventional, except when the system is KC_{24}. The closed path in reciprocal space is $\Gamma \rightarrow {}_5A \rightarrow {}_5H \rightarrow {}_5K \rightarrow {}_5\Gamma \rightarrow {}_5M \rightarrow {}_5\Lambda \rightarrow {}_3$ H, where the numbers indicate the divisions within each branch. The scaled coordinates of the (high-symmetry) points within the BZ are $\Gamma \equiv (0, 0, 0)$, $A \equiv (0, 0, 12)$, $H \equiv (-^1/_3, {}^2/_3, {}^1/_2)$, $K \equiv (-^1/_3, {}^2/_3, 0)$, $M \equiv (0, {}^1/_2, 0)$, $\Lambda \equiv (0, {}^1/_2, {}^1/_2)$.

The band-structure thus obtained is shown in Figure 9. The very localized character of the K core states gives rise to very flat bands, with virtually no dispersion throughout the Brillouin zone. The NH_3 MOs are also characterized by almost negligible dispersion, with the possible exception of the higher-energy states, which are involved in the coordination to K^+ and have more diffuse nature. As expected, the fe band is well separated from the highest bonding MO of NH_3 and its dispersion is within 2 eV. The top of this band (at H) defines the Fermi energy of the system, though some of the empty states (predominantly antibonding states of NH_3) do occasionally cross it and could in principle become partially occupied. It is interesting to notice that the dispersion of the fe band perpendicular to the plane defined by the N atoms (e.g., along the $\Gamma \rightarrow$ A branch) is relatively large, but the first empty state becomes well separated from the fe band. This may be indicative of the presence of weak interactions between a layer and its periodic replicas in the *z* direction, consistent with their reasonably short separation (∼6.65 Å). This effect is likely to depend substantially on the layer separation in the *z* direction. Indeed it was found that increasing *c* from 6.65 to 10 Å decreases the energy separation

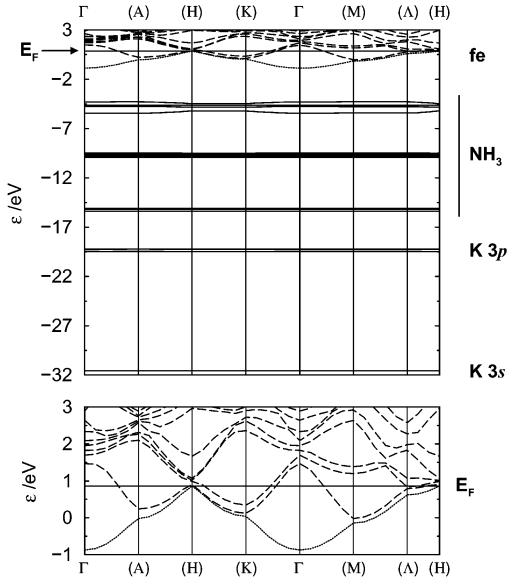

Figure 9. Band-structure of the free $K(NH_3)_4^+ \cdot e^-$ layer. E_F indicates the Fermi energy. Filled and empty states are represented by continuous and long-dashed lines, respectively. The dotted line is the floating-electron (fe) band. The region near the Fermi energy is reproduced in the lower panel. Band assignments (upper panel, right) have been determined by direct inspection of the relevant single-particle charge density distribution plots.

between the fe band and the first empty band at Γ (which can be regarded as a rough estimate by excess of the overall dispersion of the fe band) from ∼2.3 to ∼1.6 eV.

In summary, it has been shown that the HOMO of the two-dimensional $K(NH_3)_4^+ \cdot e^-$ hexagonal crystal forms an extended state characterized by percolating paths with wide oscillations in the charge density, a situation similar to that which is observed in expanded metals. In addition, this state gives rise to a narrow band and its metallic character is thus likely to be strongly affected by electronic correlations which can eventually lead to a transition to the insulating state. In any case, despite extending throughout the lattice, such a state is likely to be characterized by a poor (or possibly zero, depending on the importance of correlation effects) electric conductivity, and transfer of electronic charge from a metallic conductive path (i.e., the graphite layers of a GIC) would therefore result in an overall decrease of the in-plane conductivity. The reduction of the free carrier density in the metallic moiety and the trapping of electrons in a low mobility state would contribute jointly to hindering the free motion of the electrons.

The main results of this section will be used in the following discussion to interpret the electronic structure of the full $K(NH_3)_4C_{24}$ GIC. Within a "rigid-band" picture of the intercalation process, the global band-structure of the GIC may be sketched, starting from a simple superposition of the band-structures of the graphitic sheets ($C_{24}^{(-)}$) and the $K(NH_3)_4^{(+)}$ intercalate layer. Under the assumption of *complete* charge back-transfer from the carbon atoms to the $K-NH_3$ layer, this amounts to summing up the band-structure plots of the C_{24} framework and $K(NH_3)_4$, both as neutral species. As will be shown in the next section, the rigid-band model does indeed provide a convenient reference framework from which to make sense of the electronic structure of the intercalate system, particularly in discussing the nature and properties of bands in the vicinity of the Fermi energy. Important deviations from this simple approach to the true electronic structure are, however, anticipated in connection with frequent crossings between C and K,NH_3 bands, and, possibly, with an *incomplete* [C] → [K,NH_3] charge transfer.

IV. Electronic and Optical Properties of the $K(NH_3)_4C_{24}$ GIC

a. Band-Structure of C_{24} and $K(NH_3)_4C_{24}$. Calculations on the full $KC_{24}(NH_3)_4$ GIC were performed on the optimized structure[10] using Vanderbilt ultrasoft pseudopotentials with semicore 3*s* and 3*p* states of K included among the valence states. Calculations were also carried out on the empty C_{24} framework, with the ions frozen in the optimized positions determined for the full intercalate. This system thus corresponds to a hypothetical *stage-I* (AAA stacking[37]) compound with vertical separation between graphene sheets $I_c = 6.65$ Å. Band-structures were computed using the same details as in the previous section and they are shown in Figure 10.

The position of the fe band in the plot was estimated by direct comparison with the band-structure of the $K(NH_3)_4$ layer (Figure 9) by taking the 3*s* band of K as reference, which also allowed the approximate position of the K 3*s* and NH_3 bands to be located. From this rough estimate of the energy window (which, not unexpectedly, was found to be located in the close vicinity of the Fermi energy, assuming this to coincide with the top of the valence band), we obtained more detailed information on the band dispersion by examining single-particle charge densities ($\rho_{i\mathbf{k}}(\mathbf{r}) = \phi_{i\mathbf{k}}^*(\mathbf{r})\phi_{i\mathbf{k}}(\mathbf{r})$) for several states at various points in the Brillouin zone within the energy range predicted by the rigid-band model, and we singled out at each of these **k**-points the energy of the state whose density distribution resemble more closely the fe state in $K(NH_3)_4$ (Figure 7). In practice, only one state at each **k**-point turned out to have a nonnegligible density contribution in the $K-NH_3$ layer region, the nearby states being located exclusively on the graphite sheets, though a clear tendency of the fe state density to extend toward the C layers (associated with a direct mixing with the C orbitals) was often observed. The asterisks in the lower right panel of Figure 10, which represent the position of the fe band in the intercalate, can be used to estimate its dispersion and, as in the case of the $K(NH_3)_4$ layer, this was found to be no larger than 2 eV, with a probable band maximum at H and a minimum at Γ.

These results indicate that the nature of the extended state in the GIC is essentially the same as in the free $K-NH_3$ layer and justify the use of the rigid-band approach as an approximate way to predict the global band-structure of the intercalate from those of its hypothetical constituents. The issue of the actual occupation of the fe band is however more delicate. Our calculations are based on the solution of an independent set of Kohn−Sham equations for each **k**-point included in the Brillouin zone sampling. This yields an fe state which is *not* occupied anywhere in the Brillouin zone, and therefore never contributes to the (ground-state) Kohn−Sham potential. On the other hand, the graphitic bands near the Fermi energy are characterized by wide dispersion and the top of the valence band at a given **k**-point (e.g., at H, Figure 10) may be well above the energy of the fe state at another point (e.g., Γ). This suggests that the fe band may indeed be at least partially occupied, as schematically sketched in Figure 11, although this conclusion relies on the strong assumption that the Fermi energy does not shift downward appreciably in consequence of the charge redistribution among the various bands in its neighborhood. This effect, as well as the possible importance of other intrinsic limitations of conventional density functional approaches in the present context, will be be briefly addressed in Sections IIIc and IV.

b. Optical Properties of $K(NH_3)_4C_{24}$. The most convincing argument in favor of the charge back-transfer from graphite

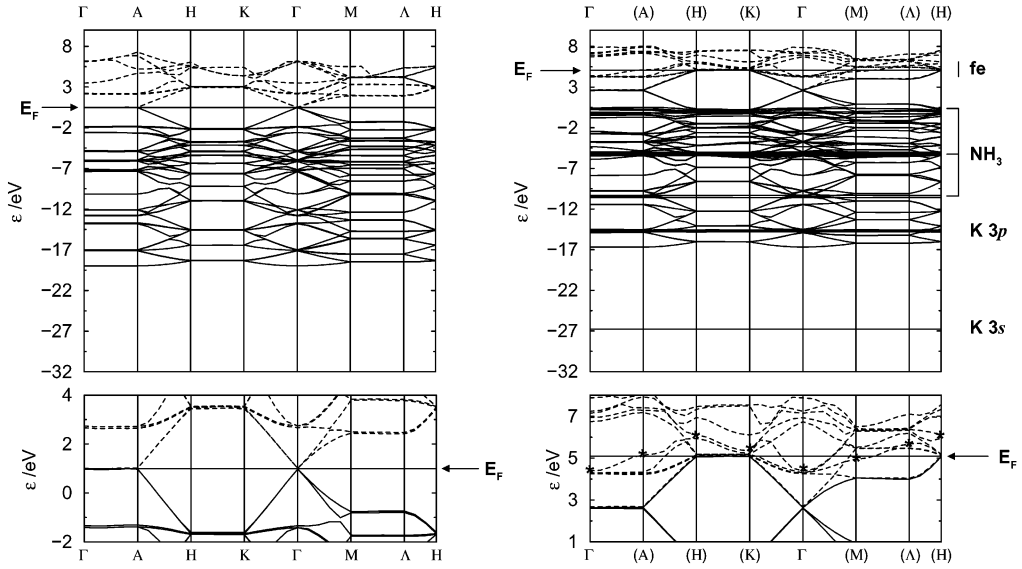

Figure 10. Band-structure of C_{24} (left) and $K(NH_3)_4C_{24}$ (right). Details are as in Figure 9. In the lower panel of $K(NH_3)_4C_{24}$, the asterisks indicate the energy of the fe band, which has been determined by direct inspection of the single-particle charge density at the points indicated. The approximate energy of the K, NH_3, and fe bands have been estimated by comparison with Figure 9, taking the K 3*s* states as reference. See text for explanation.

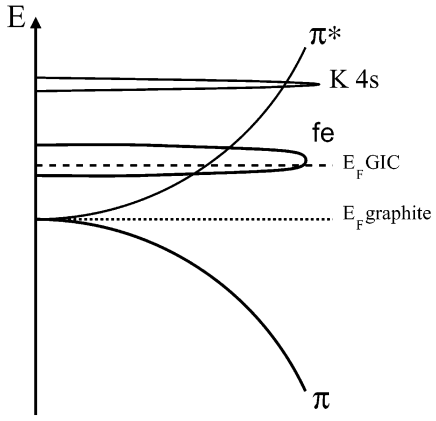

Figure 11. Hypothetical mechanism for the occupation of the fe band in a model GIC. The carbon layer bands are conventionally labeled as in clean graphite. Electrons are transferred from K 4*s* to π^* upon intercalation, therefore increasing the Fermi energy with respect to graphite. The formation of an fe state gives rise to a narrow band at lower energy with respect to K 4*s*, possibly partially below the Fermi energy. Under these circumstances *back-transfer* of electron charge from π^* to the intercalate $K-NH_3$ layer can occur.

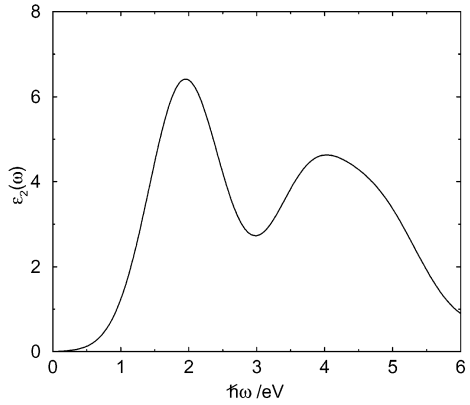

Figure 12. Calculated imaginary part of the dielectric function $\epsilon_2(\omega)$ for $K(NH_3)_4C_{24}$. Non-spin polarized insulating system, 4 **k**-point BZ sampling, 136 (67 empty) bands.

bands to the intercalant layer in GICs of composition $K(NH_3)_xC_{24}$, with $x \simeq 4$, has been proposed on the basis of measurements of *c*-face optical reflectance carried out on samples of compositions $x = 0$, 1.49, 4.11, 4.38 in the photon energy range 0.5−6 eV.[2,4] The imaginary part of the dielectric function computed from these data is characterized by a rapid decrease with increasing energy at low ω (up to ∼1.5 eV) typical of free-carrier (*intra* band) absorption, followed by an upturn which marks the transition to the *inter* band excitation region. A broad feature between ∼2.5 and 6 eV has also been observed in pristine graphite[38] and identified[39] with transitions between carbon π and π^* states near the M point (see Figure 14). In the vicinity of the $\pi-\pi^*$ interband threshold, samples of composition $x =$ 4.11 present a very intense and narrow non graphitic feature (at $\omega = 1.85$ eV). Narrow bands in the electronic absorption region have not been observed in any other GICs, though a band with similar width has been reported for potassium−ammonia solutions at $\omega \simeq 0.8$ eV. This band has been associated with 1*s* → 2*p* transitions induced between hydrogenic states describing an electron trapped in a spherical cavity of ∼6 Å diameter. Theoretical studies of the solvated electron in potassium−ammonia solutions[40] suggest that the corresponding absorption band energy increases with decreasing cavity size, though the presence of the C layers may complicate quantitative estimates of the frequency upshift.

The calculations described above provide strong support for this picture, predicting the occurrence of a solvated electron state in the intercalant layer that, though delocalized over the lattice, presents large inhomogeneities, with regions of high electron density localized in irregular "pockets" of ∼1.5 Å diameter (similar to the situation represented in Figure 7). It is therefore interesting to asses whether more quantitative information can be obtained from the above calculations, in particular if a calculated absorption spectrum can reproduce the experimentally observed features, and, provided this is the case, if an *unambiguous* assignment can be made of a particular absorption band to the fe state in the intercalant.

The response of the electronic system to an external electric field varying with time

$$\mathbf{E}(t) = \sum_n \mathbf{E}(\omega_n) e^{-i\omega_n t} \tag{4}$$

(where the sum extends over positive and negative frequencies

ω_n) manifests itself in the occurrence of a time-dependent polarization[41]

$$\mathbf{P}(t) = \sum_n \mathbf{P}(\omega_n) e^{-i\omega_n t} \tag{5}$$

At the linear response level,[42] the polarization is given by

$$P^{\alpha\beta} = \chi_I^{\alpha\beta}(-\omega;\omega) E^{\beta}(\omega) \tag{6}$$

where the superscripts indicate Cartesian components, and $\chi_I^{\alpha\beta}$ is the *linear susceptibility* related to the dielectric function by $\epsilon^{\alpha\beta}(\omega) = \epsilon_1^{\alpha\beta}(\omega) + i\epsilon_2^{\alpha\beta}(\omega) = 1 + 4\pi\chi_I^{\alpha\beta}(-\omega;\omega)$. The imaginary part of the dielectric function is given by

$$\epsilon_2^{\alpha\beta}(\omega) = \frac{e^2}{\hbar\pi m^2} \sum_{nm} \int_{\mathrm{BZ}} \mathrm{d}\mathbf{k} f_{nm} \frac{p_{nm}^{\alpha}(\mathbf{k}) p_{nm}^{\beta}(\mathbf{k})}{\omega_{mn}^2} \delta(\omega - \omega_{mn}(\mathbf{k})) \tag{7}$$

where p_{nm} are momentum matrix elements, $f_{mn} = f_m - f_n$, with f_i the Fermi occupation factor which is nonnegligible only if one of the two levels is occupied and the other empty, and the frequency difference is defined as $\omega_{mn}(\mathbf{k}) = \omega_m(\mathbf{k}) - \omega_n(\mathbf{k})$, where $\hbar\omega_n$ is the energy of the band n at wave-vector $\mathbf{k}$. ϵ_2 can therefore be estimated from a summation over the occupied and a (possibly very large) number of empty states.

A non-spin polarized calculation was carried out on $K(NH_3)_4C_{24}$ including 67 empty states (for a total of 136 Kohn−Sham orbitals for each **k**-point) computed from the same self-consistent Kohn−Sham ground-state potential used in the calculations on this system previously described, and the imaginary part of the dielectric function was determined as an average in the *ab* plane for radiation incident along the *c* axis. The Fermi factors were determined at each **k**-point by considering a level as (fully) occupied if its energy lays below the Fermi energy, given by the top of the valence band ("π*") and labeled E_F in Figure 10 (right panel). In this way, occupation of the fe band is imposed artificially within the portion of the Brillouin zone where the energy of the fe band is lower than the top of the (graphitic) valence band.

The imaginary part of the dielectric function is related to the optical conductivity σ by $\sigma(\omega) = \omega\epsilon_2/4\pi$.[43] The low-frequency domain of σ can be assumed to have the Drude form $\sigma(\omega) = \sigma(0)/(1 - i\omega/\tau)$, where $\sigma(0)$ is the DC conductivity and τ is the Drude damping (or lifetime broadening, whose value, typically ranging from 0.02 to 0.08 eV, has been set here to 0.05 eV). In the present calculations, a value of $\sigma(0) = 0$ is assumed, thus effectively removing the free-carrier contribution to conductivity and treating the system as an insulator. The main advantage of this choice is the removal of the Drude peak at $\omega \rightarrow 0$, which facilitates the identification of features in the intermediate energy region of interest. The calculated spectrum (Figure 12) is dominated by two main features in the 1−6 eV region, a sharp peak at ∼1.95 eV, and a broader band from 3 to 6 eV. Comparison with experimental spectra[4] (in particular with those at the closest composition, $x = 4.11$) shows very good agreement with regard to the lowest energy peak, with possibly a slight underestimate of its absolute intensity and a more notable tendency toward broadening. The highest energy band is less well described, but its position and overall shape do again satisfactorily agree with experiment. This proves that the procedure used here is capable of reproducing the experimental data with good accuracy. The error in the position of the main peak in the ϵ_2 spectrum with regard to experiment is ∼5%, consistent with the overestimate commonly observed in DFT calculations.[44−48]

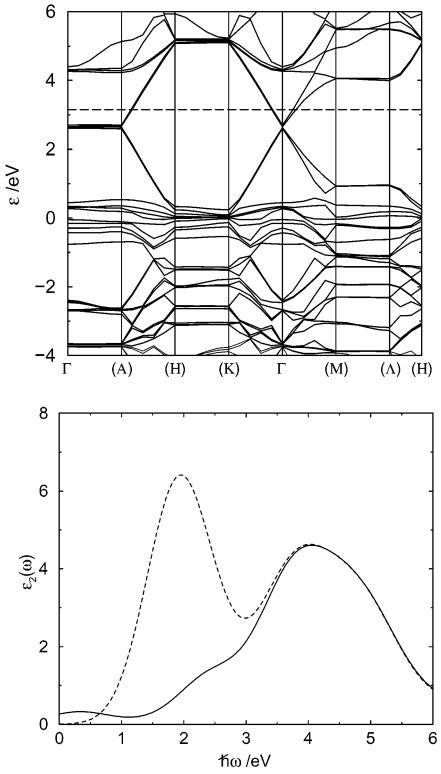

Figure 13. "Metallic" $K(NH_3)_4C_{24}$ (see text for explanation). Upper panel: Portion of the band-structure. All the states below the dashed line have occupation larger than zero. Lower panel: Calculated imaginary part of the dielectric function $\epsilon_2(\omega)$ (solid line), compared to "insulating" $K(NH_3)_4C_{24}$ (the same as in Figure 12).

c. Partial Occupation of the Kohn−Sham States and Band Assignment. A critical issue not considered so far is as to whether allowing for noninteger occupation of the Kohn−Sham states at different **k**-points (the occupation number being determined self-consistently from the whole set of **k**-points) is enough to lower the Fermi energy below the bottom of the fe band, thus preventing it from being occupied. Indeed, this was found precisely to be the case. Figure 13 shows a portion of the band-structure obtained using exactly the same specifications as in the previous non-spin polarized calculations, but considering the right (odd) number of electrons and allowing for self-consistent partial occupation. The fe band (which can be easily identified near the top of the plot) is well above the energy limit for partial occupation (dashed line) and it is therefore empty. Its promotion into the empty states results in the disappearance of the sharp peak at 1.95 eV in the complex dielectric function (Figure 13, lower panel). This fact clearly shows that this characteristic optical feature does indeed originate from electronic transitions having the fe band as starting state, and it is therefore an indirect but strong argument in favor of the charge back-transfer to the intercalate $K-NH_3$ layer in the examined GIC. It is also interesting to note that the broad group of bands between 2 and 6 eV is fully conserved in the "metallic" system, which implies that the relevant interband transitions are exclusively of graphitic character. Comparison of the calculated plot with tight-binding results and experimental data[4] for the binary compound KC_{24} further support this assignment, though band intensities, in particular that of the band at ∼2.4 eV, are markedly underestimated.

A final confirmation of the assignment of 1.95 eV band to the fe state can be obtained by comparison with the imaginary

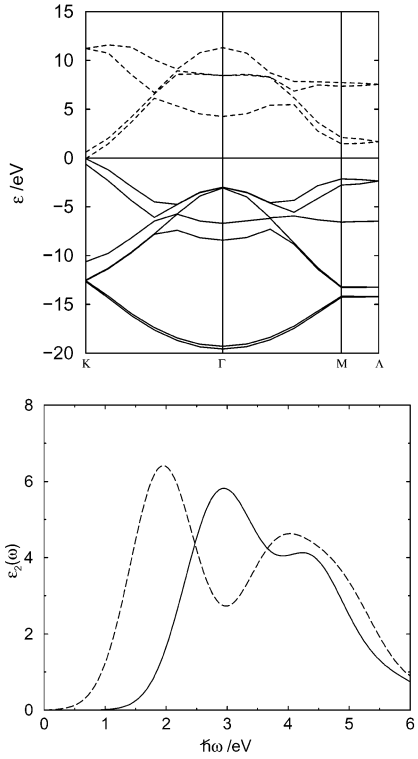

Figure 14. Band-structure (upper panel) and calculated imaginary part of the dielectric function of clean graphite (solid line) compared to $K(NH_3)_4C_{24}$ (as in Figure 12).

dielectric function computed for clean graphite. Calculations on this system were performed using the 4 atoms (2 C layers) hexagonal primitive unit cell (space group $P\,63/m\,m\,c$) of cell parameters $a = b = 2.46$ Å, $c = 6.80$ Å, $\gamma = 120°$.[51] The Brillouin zone was sampled using a $5 \times 5 \times 5$ (5 **k**-points) homogeneous Monkhorst-Pack mesh. The band-structure is shown in the upper panel of Figure 14, where the Tatar-Rabii[52,53] convention has been adopted in labeling the high-symmetry points (in reciprocal scaled units K ≡ ($^1/_3$, $^2/_3$, 0), M ≡ (0, $^1/_2$, 0) and Λ ≡ (0, $^1/_2$, $^1/_2$)). The corresponding dielectric constant (Figure 14, lower panel) was computed using an extended set of 38 **k**-points and summing over 40 empty states. The plot is now dominated by a strong peak at ∼3 eV (which presumably replaces the shoulder in metallic $K(NH_3)_4C_{24}$) and by the second usual feature at ∼4.5 eV. The total absence of the 1.95 eV peak is again evident.

V. Summary and Discussion

The existence of an extended electronic state in the $K-NH_3$ intercalate layer in the GIC $K(NH_3)_4C_{24}$ has been demonstrated on the basis of conventional density functional theory generalized gradient corrected calculations. The origin of this state has been related to the facility with which K atoms ionize upon coordination to four NH_3 molecules. This process results in the K 4*s* electron being promoted to a very diffuse state extending in the outer region of the $K(NH_3)_4$ cluster, with the electron only loosely bound to the nearly planar $K(NH_3)_4^+$ system. The tendency of this electron to displace from the cluster center as a consequence of increasing the cluster density in the formation of a two-dimensional planar crystal leads to the formation of an extended narrow band, whose charge density appears to be characterized by large spatial fluctuations. In practice, this results in the presence of tiny high-electron-density regions connected by bridging lower density areas. This situation is conserved when the two-dimensional layer is intercalated between graphite planes. As an obvious consequence, if electron density is transferred from the C layers to the intercalant, the overall conductivity can show a measurable decrease. It is worth noticing that the poorly conductive nature of the extended band can be explained simply on the basis of spatial inhomogeneities in the extended band, possibly in addition to electron correlation effects (which, of course, cannot be either ruled out or confirmed by the present calculations).

The problem of the actual occupation of the extended band is rather delicate. The energy of this electronic state lies in close proximity to the Fermi energy at several points within the Brillouin zone. According to the above calculations, occupation is brought about only if the system is treated as an insulator (i.e., if the restriction $f_i = 0$ or 1 is imposed), which has the effect of keeping the Fermi energy high enough for the fe band to occasionally cross it. In this case, the calculated imaginary dielectric function agrees remarkably well with the experimental data for GICs of similar composition, while other graphitic features persist in the spectrum, irrespective of whether the fe band is occupied or not. Therefore, the work presented here provides strong support to the link between the sharp peak in the imaginary dielectric function of $K(NH_3)_xC_{24}$ and the occurrence of an insulating localized state in the intercalate for compositions $x \simeq 4$, which has so far been justified in the literature[4,2] only in terms of its analogy with a corresponding feature recorded in $K-NH_3$ solutions.

On the other hand, a "proper" treatment of the full intercalate system, which, allowing for partial occupation of the Kohn−Sham states, accounts for changes in band energies brought about by charge reorganizations, leads to the unambiguous conclusion that the fe band is *not* occupied. Two points should, however, be considered regarding this finding. In the first place, the fe band is always empty in all the self-consistent calculations which have been performed in this work, and its contribution is therefore not included in the self-consistent determination of the (ground-state) Kohn−Sham potential. It is well-known that the presence of *self-interaction*[14,49,50] in the *occupied* states (arising from the fact that a given electron is experiencing the *full* Kohn−Sham potential, including its own contribution) is often the main reason for erratic shifts of the empty states computed from DFT calculations. Self-interaction corrections typically result in larger energy downshifts for strongly localized states (e.g., semicore *d* states in transition metals[54−59]) with respect to more diffuse ones. In this specific case, the self-interaction would affect the π^* and the fe bands in different amounts, owing to the very delocalized nature of the graphite bands and the high localization of the fe one. It is therefore not unlikely that correcting for self-interaction would result in a larger stabilization of the (empty) fe band with respect to the graphitic bands, increasing the chances for it to become partially (or fully) occupied.

Also, it should be remarked that the calculations described here have addressed only the optimized structure of the intercalate, while, on the other hand, the results of ref 10 indicate the existence of an extremely rich internal dynamics of the $K-NH_3$ layers at finite temperatures. These effects may of course in turn affect the electronic properties of the intercalate with respect to the 0 K limit. In particular, graphite layer expansion, liquidlike diffusion and flipping of the $K(NH_3)_4^+$ clusters and rotation of the NH_3 molecules may all contribute to the relative stability of bands in the vicinity of the Fermi energy, and they may therefore have a role in the above discussions. The results presented here remain nevertheless a convenient starting point for a more detailed investigation of

the connection between electronic properties and ion dynamics in $K-NH_3$ GICs.

Finally, it is interesting to address, at a purely qualitative and speculative level, the issue of the metal−insulator transition observed at $x > 4$. Under the widely accepted assumption[2,4,11] that increasing the number of NH_3 molecules in the intercalate promotes back-transfer of charge to the extended band in the $K-NH_3$ layer, and supposing that the general properties of this band remain essentially unchanged with respect to $x = 4$, the metal-nonmetal transition can be interpreted as a change in its charge distribution from a "tiny-pocket" (discrete) to a "winding channel" (continuous) regime. In this limit, the fe band would really look like a metallic band, and the conductivity should therefore start to increase again, as is indeed observed in the region $x = 4-4.5$, in concommitance with the disappearance of the sharp 1.85 eV peak in the complex dielectric function.[4] However, the presence of strong electron correlation effects would presumably prevent the system from manifesting full metallic conductivity, which could help to explain why the decrease in relative resistance at this composition range is so small with respect to the maximum at $x = 4$.

Acknowledgment. We thank D. E. Manolopoulos and M. C. Payne for useful comments. L.B. is grateful to the Queen's College, Oxford, for the award of a Florey EPA Studentship. Computing facilities were provided by the Oxford Supercomputing Centre and the EPSRC UKCP grant.

References and Notes

(1) Thompson, J. C. *Electrons in Liquid Ammonia*; Clarendon Press: Oxford, 1976.
(2) Huang, H. H.; Fan, Y. B.; Solin, S. A.; Zhang, J. M.; Eklund, P. C.; Heremans, J.; Tibetts, G. *G. Solid State Commun*. **1987**, *64*, 443.
(3) Dresselhaus, M. S.; Dresselhaus, G. *Adv. Phys*. **1981**, *30*, 139.
(4) Zhang, J. M.; Eklund, P. C.; Fan, Y. B.; Solin, S. A. *J. Phys. IV* **1991**, *1*, 311.
(5) Edwards, P. P. *J. Supercond*. **2000**, *13*, 933.
(6) Wasse, J. C.; Hayama, S.; Skipper, N. T.; Benmore, C. J.; Soper, A. K. *J. Chem. Phys.* **2000**, *112*, 7147.
(7) Tongraar, A.; Hannongbua, S.; Rode, B. M. *Chem. Phys*. **1997**, *219*, 279.
(8) Deng, Z.; Martyna, G. J.; Klein, M. L. *Phys. Rev. Lett*. **1993**, *71*, 267.
(9) Martyna, G. J.; Klein, M. L. *J. Chem. Phys*. **1992**, *96*, 7662.
(10) Bernasconi, L.; Madden, P. A. *J. Phys. Chem. B* **2002**, *106*, 1161.
(11) Walters, J. K.; Skipper, N. T.; Soper, A. K. *Chem. Phys. Lett*. **1999**, *300*, 444.
(12) Kohn, W.; Sham, L. *J. Phys. Rev*. **1965**, *140*, A1133.
(13) Hohenberg, P.; Kohn, W. *Phys. Rev*. **1964**, *136*, B864.
(14) Parr, R. G.; Yang, W. *Density Functional Theory of Atoms and Molecules*; Oxford University Press: Oxford, 1989.
(15) Perdew, J. P.; Wang, Y. *Phys. Rev. B* **1991**, *45*, 13244.
(16) Hamann, D. R.; Schliiter, M.; Chiang, C. *Phys. Rev. Lett*. **1979**, *43*, 1494.
(17) Hamann, D. R. *Phys. Rev. B* **1989**, *40*, 2980.
(18) Bachelet, G. B.; Hamann, D. R.; Schliiter, M. *Phys. Rev. B* **1982**, *26*, 4199.
(19) Vanderbilt, D. *Phys. Rev. B* **1990**, *41*, 7892.
(20) Kleinman, L.; Bylander, D. M. *Phys. Rev. Lett*. **1982**, *48*, 1425.
(21) Payne, M. C.; Teter, M. P.; Allan, D. C.; Arias, T. A.; Joannopoulos, J. D. *Rev. Mod. Phys*. **1992**, *64*, 1045.
(22) We used the codes CASTEP 3.9 and CASTEP 4.2, Academic versions, licensed under the UKCP-MSI Agreement, 1999.
(23) Kresse, G.; Furthmiiller, J. *Phys. Rev. B* **1996**, *54*, 11169.
(24) Remler, D. K.; Madden, P. A. *Mol. Phys*. **1990**, *70*, 921.
(25) Monkhorst, H. J.; Pack, J. D. *Phys. Rev. B* **1976**, *13*, 5188.
(26) Marzari, N.; Vanderbilt, D. *Phys. Rev. B* **1997**, *56*, 12847.
(27) Silvestrelli, P. L.; Marzari, N.; Vanderbilt, D.; Parrinello, M. *Solid State Commun*. **1998**, *7*, 107.
(28) Silvestrelli, P. L. *Phys. Rev. B* **1999**, *59*, 9703.
(29) Bernasconi, L.; Madden, P. A. *J. Mol. Struct*. (*THEOCHEM*) **2001**, *544*, 49.
(30) Ghosez, P.; Gonze, X *J. Phys.*: *Condens. Matter* **2000**, *12*, 9179.
(31) Vuilleumier, R.; Sprik, M. *J. Chem. Phys*. **2001**, *115*, 3454.
(32) Bernasconi, L.; Madden, P. A.; Wilson, M. *Phys. Chem. Commun.* **2002**, 1.
(33) Stacy, A. M.; Johnson, D. C.; Sienko, M. J. *J. Chem. Phys*. **1982**, *76*, 4248.
(34) Stacy, A. M.; Sienko, M. *J. Inorg. Chem*. **1982**, *21*, 2294.
(35) Kohanoff, J.; Buda, F.; Parrinello, M. *Phys. Rev. Lett*. **1994**, *23*, 3133.
(36) Fois, E.; Selloni, A.; Parrinello, M. *Phys. Rev. B* **1989**, *39*, 4812.
(37) Greenwood, N. N.; Earnshaw, A. *Chemistry of the Elements*; Pergamon: Oxford, 1984.
(38) Taft, E. A.; Phillip, H. R. *Phys. Rev*. **1965**, *138*, 195.
(39) Johnson, L. G.; Dresselhaus, G. *Phys. Rev. B* **1973**, *7*, 2275.
(40) Jortner, J. *J. Chem. Phys*. **1959**, *30*, 389.
(41) Hughes, J. L. P.; Sipe, J. E. *Phys. Rev. B* **1996**, *53*, 10751.
(42) Sipe, J. E.; Ghahramani, E. *Phys. Rev. B* **1993**, *48*, 11705.
(43) Ashcroft, N. W.; Mermin, N. D. *Solid State Physics*; Holt-Saunders: Philadelphia, 1976.
(44) Baroni, S.; Resta, R. *Phys. Rev. B* **1986**, *33*, 7017.
(45) Levine, Z. H.; Allan, D. C. *Phys. Rev. B* **1991**, *43*, 4187.
(46) Levine, Z. H.; Allan, D. C. *Phys. Rev. B* **1991**, *44*, 12781.
(47) Levine, Z. H.; Allan, D. C. *Phys. Rev. Lett*. **1989**, *63*, 1719.
(48) Levine, Z. H.; Allan, D. C. *Phys. Rev. Lett*. **1991**, *66*, 41.
(49) Fois, E. S.; Penman, J. I.; Madden, P. A. *J. Chem. Phys*. **1993**, *98*, 6352.
(50) Goedecker, S.; Umrigar, C. *J. Phys. Rev. A* **1997**, *55*, 1765.
(51) McKie, D.; McKie, C. *Essentials of Crystallography*; Blackwell Scientific: Oxford, 1986.
(52) Tatar, R. C.; Rabii, S. *Phys. Rev. B* **1982**, *25*, 4126.
(53) Trickey, S. B.; Miiller-Plathe, F.; Diercksen, G. H. F. *Phys. Rev. B* **1992**, *45*, 4460.
(54) Schröer, P.; Kruiiger, P.; Pollmann, J. *Phys. Rev. B* **1993**, *47*, 6971.
(55) Rohlfing, M.; Kruiiger, P.; Pollmann, J. *Phys. Rev. Lett*. **1995**, *75*, 3489.
(56) Vogel, D.; Kriiger, P.; Pollmann, J. *Phys. Rev. B* **1995**, *52*, R14316.
(57) Vogel, D.; Kruiger, P.; Pollmann, J. *Phys. Rev. B* **1996**, *54*, 5495.
(58) Rohlfing, M.; Kriiger, P.; Pollmann, J. *Phys. Rev. B* **1998**, *57*, 6485.
(59) Vogel, D.; Kriiger, P.; Pollmann, J. *Phys. Rev. B* **1998**, *58*, 3865.